Water Vapor Absorption in the Clear Atmosphere of an exo-Neptune

Jonathan Fraine[1,2,3], Drake Deming[1,4], Bjorn Benneke[3], Heather Knutson[3], Andrés Jordán[2], Néstor Espinoza[2], Nikku Madhusudhan[5], Ashlee Wilkins[1], Kamen Todorov[6]
composition
(1) University of Maryland Department of Astronomy
(2) Pontificia Universidad Católica de Chile, Instituto de Astrofísica
(3) California Institute of Technology Division of Geological & Planetary Sciences
(4) NASA Astrobiology Institute's Virtual Planetary Laboratory
(5) University of Cambridge, Institute of Astronomy
(6) ETH Zürich, Department of Physics

Transmission spectroscopy to date has detected atomic and molecular absorption in Jupiter-sized exoplanets, but intense efforts to measure molecular absorption in the atmospheres of smaller (Neptune-sized) planets during transits have revealed only featureless spectra[1,2,3,4]. From this it was concluded that the majority of small, warm planets evolve to sustain high mean molecular weights, opaque clouds, or scattering hazes in their atmospheres, obscuring our ability to observe the composition of these atmospheres[1,2,3,4,5]. Here we report observations of the transmission spectrum of HAT-P-11b (~4 Earth radii) from the optical to the infrared. We detected water vapour absorption at 1.4 micrometre wavelength. The amplitude of the water absorption (approximately 250 parts-per- million) indicates that the planetary atmosphere is predominantly clear down to ~1 mbar, and sufficiently hydrogen-rich to exhibit a large scale height. The spectrum is indicative of a planetary atmosphere with an upper limit of ~700 times the abundance of heavy elements relative to solar. This is in good agreement with the core accretion theory of planet formation, in which gas giant planets acquire their atmospheres by directly accreting hydrogen-rich gas from the protoplanetary nebulae onto a large rocky or icy core[6].

We observed transits of HAT-P-11b[7] (M_p = 25.8 ± 2.9 $M_\oplus$; R_p = 4.37 ± 0.08 $R_\oplus$; T_{eq} = 878 ± 50 K) in a joint Hubble-Spitzer program. Our Hubble observations comprised 1.1-1.7 micrometre grism spectroscopy using the Wide Field Camera 3 (WFC3) in spatial scanning mode. We also integrated these data over wavelength to produce WFC3 photometry[1,2,3,4,8]. Our Spitzer observations comprised photometry during two transits per 3.6 & 4.5 micrometre band of the IRAC instrument[9]. Because the planet lies in the Kepler field[10], precision optical photometry (~642nm) was obtained simultaneously with our Spitzer observations, although not simultaneously with our Hubble observations. Table 1 summarizes specific details of our observations and Figure 1a shows our transit photometry and model fits. Because HAT-P-11 is an active planet-hosting star[11,12,13], we show that starspots on

the stellar surface are not sufficiently cool, nor sufficiently prevalent, to mimic the effect of water vapour absorption in the planet[14]. Our simultaneous Spitzer and Kepler photometry was critical to defining the temperature of the starspots that could otherwise, potentially mimic the effect of water vapour absorption in the planetary atmosphere.

HAT-P-11b crosses starspots on virtually every transit [12,13], as seen prominently Figure 1a. Our WFC3 photometry has the sensitivity to detect starspot crossings[2], but none were observed when HST observed the system. Our WFC3 observations contain large temporal gaps because Hubble passes behind the Earth[1,2,3,4,8,15], but not during the transit. Therefore, *un*occulted starspots, rather than occulted ones, potentially affect our transmission spectrum[16,17]. When the planet blocks unspotted portions of the stellar photosphere, the absorption lines in cool unocculted spots become relatively more prominent[12,13].

Figure 1a shows the binned and normalised light curves of our four simultaneous Kepler-Spitzer transits and our WFC3 band-integrated light curve. We fit analytic transit light curves to all of time series with PyMC[18] to generate Markov Chain Monte Carlo (MCMC) distributions to estimate of the planetary parameters[19,20]. We re-analyzed the phased & binned Kepler data using improved limb darkening coefficients derived from stellar model atmospheres[21]. To fit the Spitzer and WFC3 transits, we hold the orbital distance and inclination constant at our Kepler-derived values. Although the uncertainties for the Kepler derived parameters were improved compared to previous studies[12,13], our purpose was to implement the updated limb darkening law and derive orbital parameters for all of our observations.

Each of the Kepler light curves obtained concurrently with our Spitzer observations show starspot crossings as deviations in the light curves between ~0.3-0.7 hours after mid-transit. The amplitude of these deviations is a function of both the area and temperature of the occulted spots [12,13]. Because the Kepler and Spitzer photometry were concurrent, the relative intensity is independent of the starspots' areas. On the other hand, because the starspots' temperature contrasts with the photosphere is a chromatic effect, the amplitude of these deviations varied with wavelength[16,17]. The spot crossings are not obvious in the Spitzer data because thermal radiation produces a much smaller contrast between the stellar photosphere and spot fluxes in the infrared than in the optical. The ratio between the Spitzer and Kepler spot crossing amplitudes constrained lower limits on the starspot temperatures for the crossed starspots.

We included the relative shape of the spot crossings, sliced from each residual Kepler light curve, and scaled their amplitudes as a free parameter in our MCMC analysis with our Spitzer transits. The distributions of relative Spitzer / Kepler spot crossing amplitudes are shown in Figure 1b. The dashed black lines represent the predicted spot crossing amplitude ratio for given spot temperature contrasts. We calculated these temperatures by representing the spots using model, stellar

atmospheres at various temperatures[22]. Using $\delta\chi^2$ tests, we indirectly detected spot crossings only at 3.6 micrometres because only these Spitzer observations resulted in positive, bounded photosphere-to-spot temperature contrasts. The 4.5 micrometre Spitzer observations are consistent with zero, or a non-detection at infrared wavelengths. These measurements, especially the non-detections, imply that the starspots crossed during each transit are too hot to mimic water vapour absorption features in the planetary spectrum[12,14]. Our starspot analysis is described in the Methods section along with the distribution of Kepler spot crossing amplitudes for comparison with those observed concurrently with Spitzer.

The activity of HAT-P-11[7,11,12,13] produces variations in the total brightness of the star from spots rotating in and out of view, which will change the band-integrated transit depth measured at different epochs. If the relative stellar brightness at the epoch of each observation is known, then the transit depths can be corrected to a common value. Kepler measured the HAT-P-11's relative brightness during all four Spitzer observations, but not during our WFC3 observation. The unknown stellar brightness during this observation introduced an additional uncertainty in our estimate of the WFC3 transit depth relative to the Spitzer and Kepler observations of ±51ppm. In Figure 2, the offset between the WFC3 spectrum and the best-fit model is, ~98ppm on average.

Figure 2 shows our HAT-P-11b transmission spectrum with Kepler, WFC3, and Spitzer transits combined. We constrain the atmospheric composition using the SCARLET tool, a new evolution of the Bayesian retrieval framework described in previous studies[23,24]. Our primary results are a robust 5.1σ detection of water absorption in the WFC3 data and a 3σ upper limit on the exo-Neptune's atmospheric metallicity of ~700 times solar metallicity (the abundance of heavy elements relative to solar)[5], corresponding to a mean molecular weight of ~10.2 g/mol at the 10 mbar level (Figure 3). Transmission spectra of selected atmospheric models[23,24,25,26] are plotted for a comparison to the observations in Figure 2, with matching symbols in Figure 3. Although the significance of the water vapour detection is unaffected by uncertainties in the stellar activity, because all wavelengths in the water band are measured simultaneously, this uncertainty inhibited placing robust constraints on the methane and carbon dioxide abundance, and therefore the C/O ratio of HAT-P-11b's atmosphere[26].

Figure 3 shows that constraints on the atmospheric metallicity and cloud top pressure are correlated. Atmospheric compositional scenarios along a curved distribution agree with the data at 3σ, spanning a range of atmospheric metallicities from 1 to 700 times solar metallicity. Figure 2 shows that a representative 10,000 times solar (water-dominated) spectrum is robustly excluded by the data. The high mean molecular weight of this atmosphere would not allow the significant water absorption feature observed in the WFC3 band pass.

We found that models with atmospheric metallicities corresponding to solar metallicity require the presence of small particles hazes to simultaneously match the HST and Kepler data points. The fit to the data improves towards higher metallicities, reaching the best-fit value at 190 times solar metallicity. The presence of the water absorption in the WFC3 spectrum required that any cloud deck must be at larger than the 10-mbar pressure level (Figure 3), while the Kepler and Spitzer transit depths similarly impose a lower limit on the cloud top pressure.

The atmospheric and bulk compositions of exoplanets provide important clues to their formation and evolution. Mass and radius alone do not provide unique constraints on the bulk compositions of these planets, which are degenerate for various combinations of rock, ice, and hydrogen gas[27]. By measuring the mean molecular weight of the atmosphere using transmission spectroscopy, we can resolve these degeneracies and provide stronger constraints on the interior compositions of these planets[5,24,27,28]. Observations of water vapour dominate the shape of the infrared spectral features for warm (~1000 K) exoplanets. In contrast, the featureless transmission spectra observed for several, similarly small planets[1,2,3,4,16] ($R_p \sim 3$–$4\ R_\oplus$) imply scattering hazes, clouds, or high mean molecular weights exist in those atmospheres, obscuring absorption features[5,23,24] and limiting our ability to understand their interiors directly[5,24,27]. HAT-P-11b is the smallest and coldest planet with a measured absorption signature through transmission, allowing the estimation of its atmosphere's mean molecular weight, providing new insights into the formation history of this Neptune-mass planet[5,24,27,28,29,30].

CITATIONS

1 Knutson, H., *et al.* A Featureless Transmission Spectrum for the Neptune-Mass Exoplanet GJ 436b. *Nature*, **505**, 66-68 (2014)

2 Kreidberg, L., *et al.* Clouds in the Atmosphere of the Super-Earth Exoplanet GJ 1214b. *Nature* **505**, 69-71 (2014)

3 Knutson, H., *et al.* Hubble Space Telescope Near-IR Transmission Spectroscopy of the Super-Earth HD 97658b. http://arxiv.org/abs/1403.4602 (2014).

4 Ehrenreich *et al.* Near-infrared transmission spectrum of the warm-Uranus GJ 3470b with the Wide Field Camera-3 on the Hubble Space Telescope. http://arxiv.org/abs/1405.1056v3 (2014).

5 Moses, J., *et al.* Compositional Diversity in the Atmospheres of Hot Neptunes, with Application to GJ 436b. *Astrophys. J.* **777**, 34 (2013)

6 D'Angelo, G., Durisen, R.H., & Lissauer, J.J. Giant Planet Formation. p. 319 in Exoplanets (ed. S. Seager) in the Space Science Series of the University of Arizona Press (2010)

7 Bakos, G., *et al.* HAT-P-11b: A Super-Neptune Planet Transiting a Bright K Star in the Kepler Field. *Astrophys. J.* **710**, 1724 (2010)

8 Deming, D., *et al.* Infrared Transmission Spectroscopy of the Exoplanets HD 209458b and XO-1b Using the Wide Field Camera-3 on the Hubble Space Telescope. *Astrophys. J.* **774**, 95 (2013)

9 Fazio, G., *et al.* The Infrared Array Camera (IRAC) for the Spitzer Space Telescope. *Astrophys. J.* **154**, 10-17 (2004)

10 Borucki, W., *et al.* Kepler Planet-Detection Mission: Introduction and First Results. *Science* **327**, 977 (2010)

11 Knutson, H., Howard, A., Isaacson, H. A Correlation Between Stellar Activity and Hot Jupiter Emission Spectra. *Astrophys. J.* **720**, 1569 (2010)

12 Deming, D., *et al. Kepler* and Ground-Based Transits of the Exo-Neptune HAT-P-11b. *Astrophys. J.* **740**, 33 (2011)

13 Sanchis-Ojeda, R. & Winn, J. Starspots, Spin-Orbit Misalignment, and Active Latitudes in the HAT-P-11 Exoplanetary System. *Astrophys. J.* **743**, 61(2011)

14 Bernath, P. Water in Sunspots and Stars. *Intern. Astron. U. Symp.* **12**, 70-72 (2002)

15 Berta, Z., *et al.* The GJ1214 Super-Earth System: Stellar Variability, New Transits, and a Search for Additional Planets. *Astrophys. J.* **736**, 35 (2011)

16 Fraine, J.D., *et al.* Spitzer Transits of the Super-Earth GJ1214b and Implications for its Atmosphere. *Astrophys. J.* **765**, 127 (2013)

17 Sing, D., et al. Hubble Space Telescope transmission spectroscopy of the exoplanet HD 189733b: high-altitude atmospheric haze in the optical and near-ultraviolet with STIS. *Mon. Not. R. Astron. Soc.* **416**, 1443 (2011)

18 Patil, A., Huard, D., & Fonnesbeck, C. PyMC: Bayesian Stochastic Modelling in Python. *J. Stat. Soft.* **35**, 4 (2010)

19 Ford, E. Quantifying the Uncertainty in the Orbits of Extrasolar Planets. *Astron. J.* **129**, 1706 (2005)

20 Ford, E. Improving the Efficiency of Markov Chain Monte Carlo for Analyzing the Orbits of Extrasolar Planets. *Astrophys. J.* **642**, 505 (2006)

21 Castelli, F. & Kurucz. R. New Grids of ATLAS9 Model Atmospheres. http://arxiv.org/abs/astro-ph/0405087 (2004)

22 Husser, T.-O., *et al.* A New Extensive Library of PHOENIX Stellar Atmospheres and Synthetic Spectra. *Astron. Astrophys.* **553**, A6 (2013)

23 Benneke, B. & Seager, S. Atmospheric Retrieval for Super-Earths: Uniquely Constraining the Atmospheric Composition with Transmission Spectroscopy. *Astrophys. J.* **753**, 100 (2012)

24 Benneke, B. & Seager, S. How to Distinguish Between Cloudy Mini-Neptunes and Water/Volatile-dominated Super-Earths. *Astrophys. J.* **778**, 153 (2013)

25 Madhusudhan, N., *et al.* A High C/O Ratio and Weak Thermal Inversion in the Atmosphere of Exoplanet WASP-12b. *Nature* **469**, 64 (2011)

26 Madhusudhan, N. C/O Ratio as a Dimension for Characterizing Exoplanetary Atmospheres. *Astrophys. J.* **758**, 36 (2012)

27 Rogers, L. & Seager, S. A Framework for Quantifying the Degeneracies of Exoplanet Interior Compositions. *Astrophys. J.* **712**, 974 (2010)

28 Fortney, J., *et al.* A Framework For Characterizing The Atmospheres Of Low-Mass Low-Density Transiting Planets. *Astrophys. J.* **775**, 80 (2013)

29 Chiang, E. & Laughlin, G. The minimum-mass extrasolar nebula: in situ formation of close-in super-Earths. *Mon. Not. R. Astron. Soc.* 431, 3444-3455 (2013)

30 Hu, R. & Seager S. Photochemistry in Terrestrial Exoplanet Atmospheres. III. Photochemistry and Thermochemistry in Thick Atmospheres on Super Earths and Mini Neptunes. *Astrophys. J.* **784**, 63 (2014)

Acknowledgements. J.F., A.J., and N.E. acknowledge support from project IC120009 "Millennium Institute of Astrophysics (MAS)" of the Millennium Science Initiative, Chilean Ministry of Economy, FONDECYT project 1130857 and BASAL CATA PFB-06. N.E. is supported by CONICYT-PCHA/Doctorado Nacional. We thank Peter McCullough for his assistance in the planning and executing of our observations. We are grateful to Ian Crossfield, Laura Kreidberg, and Eric Agol for providing their open source, python code banks on their individual websites. We are also grateful for discussions with Michael Line, Jonathan Fortney, and Julianne Moses about the nature of photochemistry and interior structures. We thank the ATLAS and PHOENIX teams for providing stellar models. We also thank the SciPy and NumPy associations for providing extensive and rigorous numerical routines for an assortment of mathematical and computational techniques.

Author Contributions. J.D.F. led the data analysis for this project with contributions from D.D., H.K., N.E., A.J., and A.W. A.W. supplied HST spectral fitting routines and interpretations. N.E. and A.J. supplied python routines for MCMC, wavelet, and transit curve analyses specific to transiting exoplanets. D.D., H.K., N.E., and A.J. provided computational equipment and administration. D.D., N.M., H.K., and K.T. successfully proposed for and provided data from the HST. B.B. and N.M. provided atmospheric models and accompanying fits. B.B. provided atmospheric retrieval analysis with figures and interpretations. N.E. supplied stellar limb-darkening coefficients calculated from both ATLAS and PHOENIX models.

Author Information. Reprints and permissions information is available at www.nature.com/reprints. The authors have no competing financial interests to report. Correspondence and requests for materials should be addressed to jfraine@astro.umd.edu or jdfraine@gps.caltech.edu

FIGURES

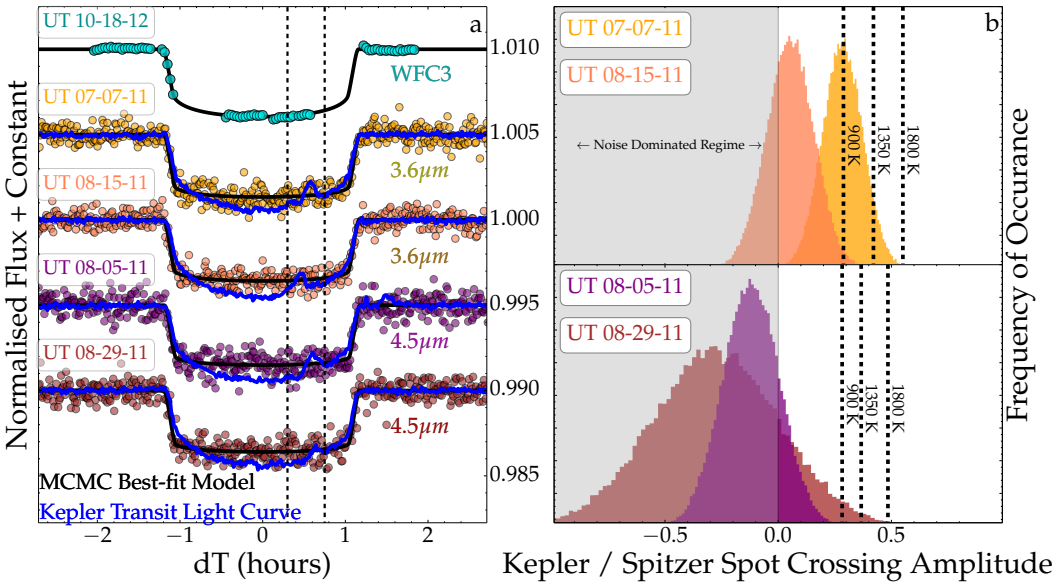

Figure 1: White-light transit curves and starspot crossing temperature estimates. a, Transit curves from HST-WFC3 and warm Spitzer, aligned in phase and shifted in flux for clarity. The four warm Spitzer transits at both 3.6 and 4.5 micrometres[9] are binned for illustration. Starspot crossings are seen as deviations near +0.5 hours in the Kepler photometry (dark blue). **b,** We estimated the starspot temperatures by dividing the Spitzer transit residuals by the Kepler transit residuals. The dashed lines represent the photosphere-to-starspot temperatures for three stellar model atmospheres[22]. Water vapour has been detected in sunspots as cool as 3000 K, corresponding to a contrast of ~1800 K here[14]. There is essentially no starspot temperature that can produce sufficiently strong water absorption to mimic our result.

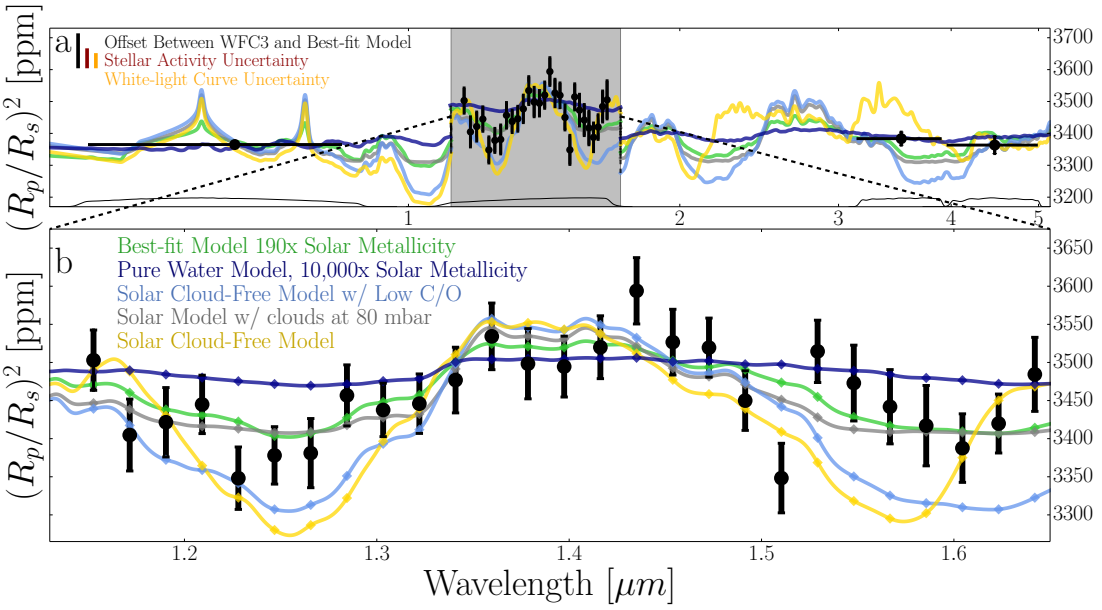

Figure 2: The transmission spectrum of HAT-P-11b. a, Our WFC3 observations show a transit depth variations in agreement with a hydrogen-dominated atmosphere. The coloured, solid lines[23,24] correspond to matching markers displayed in Fig. 3. The error bars represent the standard deviations over the uncertainty distributions. High mean molecular mass atmospheres (dark blue line) are ruled out by our observations by >3σ. The WFC3 spectrum was allowed to shift, as a unit, over these uncertainties. **b,** Detailed view of our WFC3 spectrum. For the purposes of visually comparing the spectral significance, we shifted all of the models by 98ppm in the grey region and bottom panel.

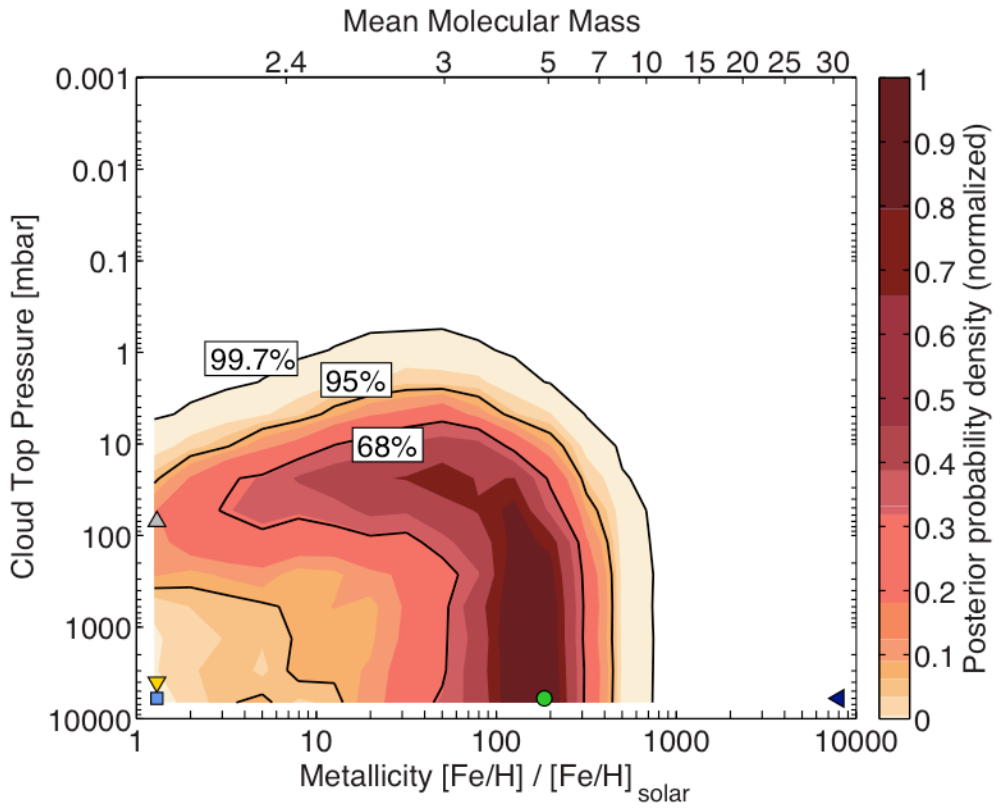

Figure 3: Spectral retrieval results of our transmission spectrum. The coloured regions indicate the probability density as a function of metallicity (the abundance of heavy elements relative to solar) and cloud top pressure derived using our Bayesian atmospheric retrieval framework[23,24]. Mean molecular weight was derived for a solar C/O ratio at 10 mbar. Black contours mark the 68%, 95%, and 99.7% Bayesian credible regions. The depth of the observed water feature in the WFC3 spectrum required the presence of a large atmospheric scale height that can self-consistently only be obtained with an atmospheric metallicity below 700 times solar at 3σ (99.7%) confidence. The atmosphere is likely predominately cloud-free at least down to the 1 mbar level. We indicate the matching models plotted in Figure 2 with coloured markers.

Date	Start Time	End Time	Observatory (Instrument)	Bandpass	Spectral Resolution	Temporal Cadence	Number of Observations
UT Jul 07, 2011	23:11:42	06:37:52	warm *Spitzer* (IRAC Channel 1)	3.6 μm	~4	0.4 s	62592
UT Aug 05, 2011	07:02:48	14:28:58	warm *Spitzer* (IRAC Channel 2)	4.5 μm	~4	0.4 s	58112
UT Aug 15, 2011	01:49:20	09:15:30	warm *Spitzer* (IRAC Channel 1)	3.6 μm	~4	0.4 s	52633
UT Aug 29, 2011	17:37:18	01:03:28	warm *Spitzer* (IRAC Channel 2)	4.5 μm	~4	0.4 s	62592
UT Oct 18, 2012	17:37:18	01:03:28	Hubble WFC3 (G141)	1.13-1.64 μm	~60 – 89	123 s	113
UT Dec 24, 2012	23:56:56	03:05:58	Hubble WFC3 (G141)	1.13-1.64 μm	~60 - 89	123 s	99

Table 1: Summary of observations.
We observed HAT-P-11b during four warm Spitzer observations, two transits at both 3.6 and 4.5 micrometres with the IRAC instrument[9], and two observations using HST WFC3 G141 grism spectrometer, spanning 1.1–1.7 micrometres. Concurrent Kepler observations were retrieved for comparison with our warm Spitzer observations, but were unavailable for our Hubble spectroscopic observations.